BEHAVIOR OF POST-INSTALLED BONDED BARS AS SHEAR REINFORCEMENT

Mathieu Fiset, Félix Antoine Villemure, Josée Bastien, Denis Mitchell

Biography:

Mathieu Fiset is an Assistant Professor at Université du Québec à Chicoutimi, Chicoutimi, Canada. He received his B. Eng., M. Sc. And Ph.D. grades from Université Laval. He is a member if the Research Center on Concrete Infrastructure (CRIB), Québec, Canada. His research interests include structural behavior, shear strengthening and bond behavior in reinforced concrete structures.

Félix-Antoine Villemure is a M. Sc. candidate in the Department of Civil Engineering at Université Laval, Quebec City, Canada. He received his B. Eng. degree from Université Laval. He is also working as a structural engineer at WSP Canada in Quebec City, Canada. His research interests include materials engineering, concrete durability, structures strengthening and bond behavior in reinforced concrete structures.

Josée Bastien is a Professor in the Department of Civil Engineering at Université Laval, Quebec City, Canada. She is a member of the Research Center on Concrete Infrastructure (CRIB), Québec, Canada. Her research interests include structural analysis, design, strengthening and damage detection in reinforced concrete and prestressed concrete structures.

Denis Mitchell, FACI, is a James McGill Professor in the Department of Civil Engineering and Applied Mechanics at McGill University. He is a member of Joint ACI-ASCE Committee 408, Bond and Development of Steel Reinforcement, and 445, Shear and Torsion. His research interests include shear behavior, seismic design, and the use of high-performance concrete.

ABSTRACT

Post-installed epoxy-bonded shear reinforcement is a promising technique to increase shear capacity of reinforced concrete structures. However, the behavior of epoxy-bonded bars largely affects the shear strengthening efficiency. To better predict the behavior of epoxy-bonded bars, a bond model is developed in this paper. This model appears to adequately predict the behavior of epoxy-bonded bars observed in experimental pull-out tests and beam loading tests. Based on numerical results, a simplified model is proposed to predict the epoxy-bonded bars stress according to the crack width. It appears that the behavior of long embedded bars is similar to stirrups, in terms of crack width and bar stress. However, a large diagonal crack is required to reach the bar yielding strength when the bar embedment length is below a transition length, which differs to stirrups. Embedment length below the epoxy-bonded bar development length leads to pullout failure and bar capacity lower than the bar yielding strength.

Keywords: Epoxy-bonded bar, bond behavior, shear reinforcement, crack width, modelling

INTRODUCTION

The brittle shear failure of the Concorde overpass in Laval, Canada in 2006 demonstrated the susceptibility of older thick slabs without shear reinforcement to brittle shear failure [1, 2]. A promising shear strengthening method for existing thick concrete slabs consists of inserting reinforcing bars into appropriately spaced pre-drilled vertical holes in the concrete and anchoring the bars with high-strength epoxy adhesive. This technique involves choosing a bar size as well as the spacing along the span and transverse to the span. Experiments have demonstrated that the shear capacity can be greatly increased using this technique [3-5]. However, it is necessary to adjust the predictions using current shear design methods for members containing conventional shear

reinforcement (stirrups installed before concrete casting) in order to predict the shear capacity of members with post-installed epoxy-bonded bars. The behavior of post-installed, epoxy-bonded, shear reinforcing bars differs from the ideally anchored cast-in-place stirrups. Assuming that the epoxy-bonded bars are ideally anchored can result in an overestimation the shear capacity by about 30% [3-5].

Fig. 1 shows the typical shear cracking pattern of a concrete member with shear reinforcement. Modern shear design codes consider that the member shear capacity is attributed to the tensile resistance of the diagonally cracked concrete, the interface shear resistance along the crack and tension in the transverse reinforcing bars [6-8]. The interface shear transfer along the inclined crack is a function of the crack width and the aggregate size. The maximum stress in the transverse reinforcing bars at the intersection of the crack with a particular reinforcing bar is a function of the crack width (related to the bar slip and the bond properties), the bar embedment length and the end anchorage conditions. In conventional reinforced concrete (RC) members with stirrups, stirrup hooks are designed so the stirrup yield strength can be developed resulting in well controlled crack widths and good aggregate interlock. For members strengthened in shear with post-installed epoxy-bonded bars, the diagonal shear crack location determines the bar embedment length, ℓ, and hence the bond strength may limit the stress developed in the transverse reinforcement. Experimental and analytical studies have shown that members reinforced with post-installed epoxy-bonded bars experience larger crack widths than members with stirrups; leading to an expected lower aggregate interlock [9]. In addition, if the crack intersects the epoxy-bonded bar near its end, then a smaller stress is developed in the bar leading to a reduced shear resistance from the transverse reinforcement.

RESEARCH SIGNIFICANCE

To better understand the behavior of members strengthened with drilled-in epoxy-bonded bars, this study compares the behavior of post-installed bonded bars to the behavior of conventional cast-in-place stirrups in terms of bond stress, bar slip, axial bar stress and development length. Bond-slip relationships are introduced into a detailed numerical model to compare the behavior of the two different types of shear reinforcement. Based on the detailed numerical results, a simplified model is proposed to predict the behavior of post-installed epoxy-bonded bars. The predictions using the detailed numerical model and the simplified model are compared with the behavior of post-installed epoxy-bonded shear reinforcement as well as the behavior of cast-in-place stirrups observed from experiments[3-5]. Therefore, the proposed models can be used to predict shear carried by epoxy-bonded shear reinforcement in RC structures.

BOND BEHAVIOR OF REINFORCING BARS

Fig. 1 and Fig. 2a show a typical diagonal shear cracking pattern for a concrete beam with stirrups and epoxy-bonded bars. The diagonal shear cracks intersect transverse reinforcing bars resulting in tension in these bars. The behavior of a transverse reinforcing bar at a crack location may be regarded as two pullout tests, one on each side of the crack (Fig. 1). The relative slip between the transverse reinforcing bar and the surrounding concrete results in opening of the crack associated with the tensile stress in the reinforcing bar. There is a relationship between the crack width and the axial bar stress at a crack location, which can be determined from the bond behavior and the anchorage condition of the bar. To determine this relationship, Fig. 2b represents the bond behavior of an epoxy-bonded bar. Typically, the bar slip is defined by the relative displacement between the bar and the surrounding concrete. Along the incremental length, dx, of a reinforced concrete element the variation of the bar slip, ds, is defined by Eq. (1) as the difference between the steel strain, ε_s, and the concrete strain, ε_c [10].

$$ds = \left(\varepsilon_s - \varepsilon_c\right) dx \tag{1}$$

From equilibrium in Fig. 2b, the relation in Eq. (2) between the concrete axial stress, f_c, the steel stress, f_s, and bond stress, τ,can be determined, where ρ_s and d_b are the reinforcement ratio and the bar diameter, respectively.

$$df_s = \frac{df_c}{\rho_s} = \frac{4}{d_b}\tau dx \tag{2}$$

Eq. (1) and (2) lead to the differential equation of bond as follows, where n is the ratio between the steel and concrete moduli (E_s / E_c).

$$\frac{d^2 s}{dx^2} - \frac{4}{d_b}\tau\left(1 + n\rho_s\right) = 0 \tag{3}$$

Balazs[10] and Lee *& al.*[11] numerically solved Eq. (3) to study the bond behavior of cracked RC members and to adequately predict the crack spacing, crack width and tension stiffening effect. Mahrenholtz[12] also used this approach to predict the behavior of RC column-to-foundation connections built with post-installed epoxy-bonded bar. A similar approach is used in this paper to study the bond behavior of epoxy-bonded shear reinforcing bars in RC members and to account for different adhesive behavior and boundary conditions. Fig. 2 illustrates the expected variation of bond stress, τ, bar slip, s, and axial bar stress, f_s, along the length of different types of embedded bars and boundary conditions.

Fig. 2c and d show a straight bar without end anchorages as for an epoxy-bonded bar. For that type of bar, the bar undergoes tension at the shear crack inducing bar axial stress, $f_{s\ell}$, at $x = \ell$ and a slip, s_ℓ. The slipping between the bar and the concrete activates the bond stress, τ, and the

axial stress, f_s, decreases along the bar. If there are no further cracks intersecting the embedded bar as illustrated in Fig. 2c, the free bar extremity ($x = 0$) is free to move ($s_0 \geq 0$) and consequently, the entire axial stress has to be transferred by bond from the bar to the surrounding concrete ($f_{s0} = 0$). Midway between two consecutives cracks ($x = 0$), the bar is pulled in two opposite directions so that the maximum axial bar stress $f_{s\ell}$ decreases between the cracks and is minimum ($f_{s0} \geq 0$) with the slip $s_0 = 0$. The resulting expected distributions of bar axial stress, slip and bond are shown in Fig. 2d and are representative for both a bar with and without end anchorages (i.e. stirrups and post-installed bonded bars).

For the hooked bar shown in Fig. 2e, the bar experiences maximum tension at the shear crack and the well-anchored extremities are typically capable of developing a significant axial stress with a relatively small displacement ($s_0 \approx 0$ and $f_{s0} > 0$) [13-16]. Fernández Ruiz *& al.*[17] proposed a model to estimate the bar slip according to the bar stress that can be used for cast-in-place hooked bars. This model results in Eq. (4) for the elastic behavior of a bar ($f_{s0} < f_y$) and proved to adequately estimate the end anchorage slip, s_0, corresponding to the bar stress, f_{s0}, for three different hooked conditions as illustrated in Fig. 3.

$$f_{s0} = \sqrt{k f_c'^{2/3} E_s \left(\frac{s_0}{d_b} \right)} \qquad (4)$$

In this equation, $k = 5$ for MPa and $k = 26.3$ for psi. In order to numerically solve Eq. (3), an embedded bar is divided in a series elements and is solved with the flow chart presented in Fig. 4. For a specified applied axial stress and slip ($f_{s\ell}$ and s_ℓ at a bar loaded end), the axial stress and bond stress as well as the slip along the bar are determined from the loaded end to the bar

extremity using Eq. (1) and (2) using appropriate material properties. The axial stress and slip determined at the bar unloaded end (f_{s0} and s_0) are compared with the boundary conditions for convergence purposes.

MATERIALS BEHAVIOR

In the context of shear strength of RC members, bar capacity is limited to the bar yield strength according to Eq. (5), where, E_s and f_y are the Young's modulus and the steel yield strength, respectively. However, in the detailed numerical analysis (Fig. 4), steel hardening is considered with Eq. (6), where E_{sh}, ε_{sh}, ε_u and f_u are the strain hardening modulus, the hardening strain (end of the yield plateau), the ultimate strain and the ultimate strength, respectively. For the concrete material, small strain is expected and the concrete behavior is considered linear elastic. If not specified, $E_c = 6900 + 3000\sqrt{f_c'}$ where f_c' is the concrete compressive strength in MPa [7] ($E_c = 1000 + 36\sqrt{f_c'}$ for f_c' in psi and E_c in ksi)

$$f_s = E_s \varepsilon_s \le f_y \tag{5}$$

$$f_s = \begin{cases} f_u + \left(f_y - f_u\right)\left(\dfrac{\varepsilon_u - \varepsilon_s}{\varepsilon_u - \varepsilon_{sh}}\right)^{E_{sh}\left(\varepsilon_u - \varepsilon_{sh}\right)/\left(f_u - f_y\right)} & \varepsilon_{sh} \le \varepsilon_s \le \varepsilon_u \\ 0 & \varepsilon_s > \varepsilon_u \end{cases} \tag{6}$$

For the detailed numerical analysis, the bond-slip relationship used for cast-in-place bars and post-installed epoxy-bonded bars is presented in Fig. 5a by a solid curve according to Eq. (7) and (8) [12, 18, 19]. This relationship is based on the following parameters: s_1 = 0.8 mm (0.032 in), s_2 = 1.8 mm (0.071 in), $s_3 = s_R$, $R = 2$, $\tau_b = \Omega_y \tau_{b0}$, $\tau_f = 0.4\tau_b$, $k_{sec} = \tau_b / s_1$, $k_1 = \left(0.8 + 20 f_R\right) k_{\text{sec}}$, k_2

= $(0.22-2f_R)k_{\sec} \geq 0$ and $s_{ref} = s_1(k_{sec}-k_2)/(k_1-k_2)$, where s_R is the ribs spacing and f_R the relative ribs area [20]. For cast-in-place reinforcing bars, $\tau_{b0} = 20 f_R^{0.8}\sqrt{f_c'}$ MPa ($\tau_{b0} = 240 f_R^{0.8}\sqrt{f_c'}$ psi) while τ_{b0} has to be experimentally determined with pullout tests for epoxy-bonded bars. The bond-slip relationship presented by a dashed curve in Fig. 5a will later be introduced for a simplified bond analysis. This parametric model was developed to consider different types of bond behavior.

$$\tau = \tau_{ref}\left(\frac{s}{s_{ref}}\right)\left[\frac{k_2}{k_1}+\left(1-\frac{k_2}{k_1}\right)\left(1+\left(\frac{s}{s_{ref}}\right)^R\right)^{-1/R}\right] \leq \tau_b \quad if\ s \leq s_2 \tag{7}$$

$$\tau = \tau_b - (\tau_b - \tau_f)\left(\frac{s-s_2}{s_3-s_2}\right) \geq \tau_f \qquad if\ s > s_2 \tag{8}$$

$$\tau_{ref} = \tau_b \frac{s_{ref}/s_1}{\frac{k_2}{k_1}+\left(1-\frac{k_2}{k_1}\right)\left(1+\left(\frac{s_1}{s_{ref}}\right)^R\right)^{-1/R}} \tag{9}$$

For high tensile strain in reinforcing bars, the bond is reduced by the lateral contraction of the bar. To take into account this effect, it is suggested to reduce as follows the bond strength by the factor Ω_y (Fig. 5b) after bar yielding occurs:

$$\Omega_y = 1-\alpha\left[1-\exp\left(-5\left(\frac{\varepsilon_s-\varepsilon_y}{\varepsilon_u-\varepsilon_y}\right)^b\right)\right] \leq 1 \tag{10}$$

Where ε_y is the yielding strain ($\varepsilon_y = f_y / E_s$), $b = \left(2 - f_u / f_y\right)^2$ and α = 0.85 for cast-in-place reinforcing bars [6, 18].

DETAILED NUMERICAL MODEL VALIDATION

Cast-in-Place Bars

To validate the detailed numerical model, the predictions made with this model are compared with the results of tests performed on cast-in-place anchorages (steel to concrete interface). Fig. 6 illustrates the results from a test carried out by Kankam[21] and Fig. 7 presents experimental results of pullout tests carried out by Shima *& al.*[22] for there different types of steel reinforcing bar (steel type SD30, SD50, SD70). The predictions made with the detailed numerical model agree very well with the experimentally determined strains, ε_s along the cast-in-place bars before and after yielding (Fig. 6b and Fig. 7c). The relationship between the applied stress, $f_{s\ell}$, and the bar loaded slip end, s_ℓ, and loaded end strain, $\varepsilon_{s(x=\ell)}$, are also well predicted by the detailed numerical model.

Epoxy-Bonded Bars

Fig. 8 shows the results from forty-three (43) pullout tests carried out by Villemure *& al.*[23] to investigate the behavior of post-installed epoxy-bonded bars with different embedment lengths, ℓ = 2 d_b, 4 d_b and 5 d_b. The reinforcing bars had a yield stress, f_y, of 456 MPa (66.1 ksi) and an ultimate strength, f_u, of 560 MPa (81.2 ksi). The tests were carried out with an average measured concrete compressive strength, f_c', of 41.6 MPa (6030 psi). All the tests failing by debonding before bar yielding enabled the determination of the epoxy adhesive bond strength (τ_{b0} = 32.5 MPa (4700 psi)).

Fig. 8b presents the bond stresses determined from the measured slips and compares these values with the predictions. The maximum capacities of the epoxy-bonded bars ($f_{s\ell,max}$) are presented in Fig. 8c and are compared with the numerical predictions. It can be seen that the bar development length, ℓ_{d0}, required to fully develop f_y is about 56 mm (2.205 in) for these tests. Also, a very good match is found between the experimental and predicted responses for $\ell = 2d_b$ (Fig. 8b and c). For bars experiencing yielding ($4d_b$ and $5d_b$), Fig. 8c shows that the numerical model predictions do not adequately predict the responses using the bond modification factor α of 0.85, typically used for cast-in-place reinforcement (Eq. (10)). The experimental results indicate that the epoxy-bonded bars with $\ell = 5d_b$ have ruptured before debonding. By using $\alpha = 0.85$, the numerical model predicts debonding of these bars and maximum capacity of about one half of the experimental capacities ($f_{smax,calc} / f_{smax,test}$ avg = 0.60, CoV = 0.44). On the other hand, the predictions omitting Ω_y ($\alpha = 0$ in Fig. 8c) overestimate the capacities of bonded bars with $\ell = 4d_b$ ($f_{smax,calc} / f_{smax,test}$, avg = 1.18, CoV = 0.43). A good match with experimental results is found in Fig. 8c with $\alpha = 0.20$ (avg = 1.04, CoV = 0.32). This suggests that the bond strength of epoxy-bonded bars is not as affected by steel yielding as cast-in-place reinforcement. This can be attributed to the increased bond strength for the epoxy-bonded bars (i.e. chemical adhesion and materials behavior [12, 24]).

SIMPLIFIED MODEL FOR EPOXY-BONDED BARS

Based on the detailed numerical model, a simplified model is developed for post-installed epoxy-bonded bars in RC structures. Fig. 9 presents the axial bar stress, the slip and the bond stress along an epoxy-bonded bar (materials properties from the tests of Villemure & *al.*[23]) for different

embedment lengths of ℓ_{d0}, $2\ell_{d0}$ and $10\ell_{d0}$, where ℓ_{d0} is the bar development length determined as follows:

$$\ell_{d0} = \frac{f_y d_b}{4\tau_{b0}} \tag{11}$$

For $\ell = \ell_{d0}$, Fig. 9 shows that the bond stress is about constant along the bar and it reaches the bond strength, τ_{b0}. Consequently, the bar slip is constant along the bar and it reaches s_1 (see Fig. 5 for the definition of s_1). For a longer embedment length of $2\ell_{d0}$, a smaller slip of about $0.2 s_1$ or less may be observed along the bar. The simplified model needs to account for the difference in behavior for short and long embedment lengths.

Plastic Behavior (P) for Short Embedment Lengths

A bar with a short embedment length has a constant bond stress along ℓ. The bond stress τ becomes independent of x and, by neglecting ε_c (much smaller than ε_s), Eq. (3) can be solved. For the free extremity boundary conditions (see Fig. 2b), the following equations can be determined, where the bond stress τ is constant along the bar and determined with the bond-slip relationship given by Eq. (7).

$$s_P(x) = s_\ell + \frac{2\tau}{d_b E_s}(x^2 - \ell^2) \tag{12}$$

$$f_{s,P}(x) = \frac{4x}{d_b}\tau \le f_y \tag{13}$$

A simplified bond stress-slip relationship may be adopted as given by Eq. (14) [25], where α_{bp} may be estimated as $\left(0.7 + 18 f_R\right)^{-1}$ (for the tested epoxy adhesive bonded bars, $\alpha_{bp} \approx 0.35$), and k_d = 1 before debonding ($s_\ell < s_2$).

$$\tau = \tau_b k_d \sqrt{1 - \exp\left(\frac{-s_\ell}{\alpha_{bp}}\right)} \tag{14}$$

When s_ℓ reaches s_2, debonding occurs and the bond stress from Eq. (14) needs to be reduced by multiply by the following coefficient.

$$k_d = 1 - 0.6\left(\frac{s_\ell - s_2}{s_3 - s_2}\right) \begin{cases} \geq 0.4 \\ \leq 1 \end{cases} \tag{15}$$

Combining Eq. (13) to (15) leads to the following equation to determine the applied bar stress, $f_{s\ell}$, according to the bar loaded end slip, s_ℓ.

$$f_{s\ell} = \frac{4\ell \tau_b k_d}{d_b} \sqrt{1 - \exp\left(\frac{-s_\ell}{\alpha_{bp}}\right)} \tag{16}$$

Elastic Behavior (E) for Long Embedment Lengths

For embedment lengths larger than $2\ell_{d0}$, a small slip is expected ($s < s_{ref}$) along the bar up to bar yielding (Fig. 9). In such cases, the bond-slip relationship is about linear (see Fig. 5) and may be expressed by Eq. (17). By neglecting ε_c, Eq. (3) can be solved to determine the slip and axial bar stress along the bonded bar.

$$\tau = k_1 s(x) \tag{17}$$

In the case of a bar with free extremity boundary conditions (i.e. bar end stress $f_{s,0}$ = 0 and bonded bar extremity is free to move, s_0 > 0, see Fig. 2b), the solution leads to the simplified model EF given by Eq. (18) and (19) as follows:

238 $$s_{EF}(x) = s_\ell \exp\left(\frac{\ell - x}{\ell_k}\right)\left[\frac{\exp(2x/\ell_k)+1}{\exp(2\ell/\ell_k)+1}\right] \quad (18)$$

239 $$f_{s,EF}(x) = s_\ell \frac{E_s}{\ell_k} \exp\left(\frac{\ell - x}{\ell_k}\right)\left[\frac{\exp(2x/\ell_k)-1}{\exp(2\ell/\ell_k)+1}\right] \le f_y \quad (19)$$

240 For a bar between two cracks, the bonded bar boundary conditions (i.e. bar stress and bar slip
241 between two cracks are respectively $f_{s,0} > 0$ and $s_0 = 0$, see Fig. 2c) lead to the model EC given
242 in Eq. (20) and (21) as follows:

243 $$s_{EC}(x) = s_\ell \exp\left(\frac{\ell - x}{\ell_k}\right)\left[\frac{\exp(2x/\ell_k)-1}{\exp(2\ell/\ell_k)-1}\right] \quad (20)$$

244 $$f_{s,EC}(x) = s_\ell \frac{E_s}{\ell_k} \exp\left(\frac{\ell - x}{\ell_k}\right)\left[\frac{\exp(2x/\ell_k)+1}{\exp(2\ell/\ell_k)-1}\right] \le f_y \quad (21)$$

245 In the previous equations, the length ℓ_k is defined as follows:

246 $$\ell_k = \sqrt{\frac{d_b E_s}{4k_1}} \quad (22)$$

247 For a large ratio of ℓ / ℓ_k (about larger than 1), the right-hand term in brackets of Eq. (18) to (21)
248 is close to 1 and the stress at the bar loaded end can simply be determined by Eq. (23), for free
249 bar extremity boundary conditions and between two cracks. Therefore, this equation gives a
250 relationship between the applied stress, $f_{s\ell}$, and the bar loaded end slip, s_ℓ, as given by:

251 $$f_{s\ell,E} = E_s \frac{s_\ell}{\ell_k} \le f_y \quad (23)$$

252 **Transition Between E and P Behaviors**

253 The transition length ℓ_t between the plastic (P) and elastic (E) behaviors is determined according
254 to the slip corresponding to yield of the bar, s_y. From Eq. (16) and (23), s_y can be determined for
255 each type of behavior, with Eq. (24) and (25) as follows:

256 $$s_{y,P} = \alpha_{bp} \ln\left(\frac{\ell^2}{\ell^2 - \ell_{d0}{}^2}\right) \quad (24)$$

257 $$s_{y,E} = \ell_k \frac{f_y}{E_s} \quad (25)$$

258 By comparing Eq. (24) and (25), the transition between the two types of behavior can be
259 evaluated using Eq. (26). Typically, ℓ_t varies between 1.3 and 2.3 ℓ_{d0} for epoxy-bonded bars.

260 $$\ell_t = \ell_{d0} \sqrt{\frac{\exp\left(\frac{\ell_k f_y}{\alpha_{bp} E_s}\right)}{\exp\left(\frac{\ell_k f_y}{\alpha_{bp} E_s}\right) - 1}} \quad (26)$$

261 Fig. 10a compares the slip s_y for different embedment lengths as well as their stress-slip
262 behavior based on the simplified model with the detailed numerical model predictions. The steel
263 properties correspond to the properties of the bars tested by Shima *& al.*[22] and Villemure *& al.*[23].
264 The transition length corresponds to the intersection between the predicted values of s_y
265 determined from elastic and plastic behavior. By looking at the numerical predictions, it can be
266 seen that a small variation of embedment length significantly affects s_y for a short embedded
267 bars ($\ell \leq \ell_t$), but the large variation of the bar slip s_y is well predicted by the plastic behavior of
268 the simplified model, $s_{y,P}$. For $\ell > \ell_t$, s_y is about the same for any embedment length and is
269 well predicted by the elastic behavior of the simplified model, $s_{y,E}$.

Fig. 10b compares the axial stress, $f_{s\ell}$, as a function of the loaded end slip, s_ℓ, predicted by the detailed numerical model and the simplified model. It can be seen that the plastic behavior of the simplified model provides accurate prediction of the behavior for $\ell < \ell_t$, while the elastic behavior of the simplified model is more appropriate for $\ell \geq \ell_t$.

BEHAVIOR OF BARS AT SHEAR CRACKS

Behavior of an Epoxy-Bonded Bars in Beams

Straight epoxy-bonded bars can exhibit bar yielding, bar rupture and bar debonding. An additional failure mode needs to be considered to account for concrete breakout. In beams, epoxy-bonded shear reinforcement can experience a concrete cone pullout failure for short embedment lengths beyond the crack locations . To consider this failure mode for an epoxy-bonded bar, Eligehausen *& al.*[26] proposed to limit the uniform bond strength as follows:

$$\tau_b \leq \frac{4.7}{d_b}\sqrt{f_c'\ell} \tag{27}$$

To consider a concrete cone failure at a crack location in a beam, the embedment length is divided into a concrete cone length, ℓ_c, and an effective embedment length $\ell - \ell_c$ as illustrated in Fig. 11 [27-29]. After the formation of the concrete cone, the load transferred to the concrete as well as the bond stress along ℓ_c can be taken as zero. The length ℓ_c is determined so that the average bond stress along $\ell - \ell_c$ respects Eq. (27). By considering Eq. (27), the average bond strength at the bar yielding τ_{by} and the development length ℓ_d can be determined from Eq. (28) and (29), respectively.

$$\tau_{by} = 1.77\sqrt[3]{\frac{f_c' f_y}{d_b}} \le \tau_{b0} \quad (28)$$

$$\ell_d = \frac{f_y d_b}{4\tau_{by}} \quad (29)$$

Axial Bar Stress at a Shear Crack

A typical shear cracking pattern in a RC member showing the intersection of an inclined crack with a transverse reinforcing bar is illustrated in Fig. 1 and Fig. 12. Typically, the angle of the shear crack, θ varies between 30° and 60° and the inclined crack spacing, $s_{m\theta}$, is about 300 mm (12 in) for members with shear reinforcement [30, 31]. The crack width typically decreases from the crack width at the surface of the concrete, w, to the crack width at the level of the bar, ω, with w being about 1.3ω [32]. At maximum shear capacity, δ is about half of ω [32-34] and the vertical displacement at a crack, u_y, is represented by Eq. (30).

$$u_y = \frac{w}{1.3}\left(\cos\theta + 0.5\sin\theta\right) \quad (30)$$

For a typical RC member where θ varies between 30° and 60°, $w \approx 1.3u_y$ and ℓ_2 can be estimated as half the vertical crack spacing and is somewhat greater 150 mm[31] (6 in ,see Fig. 12a). By neglecting the elongation of the bar between crack faces, the slippage $s_{\ell 1}$ and $s_{\ell 2}$ of a vertical bar also equals u_y (see Fig. 12b). For a given bar stress at a crack, f_{scr}, the slip on each side of the crack can be determined from Eq. (12) to (23). Three types of likely cracks in a shear strengthened RC member are illustrated in Fig. 12 with associated bar stress $f_{scr,1}$, $f_{scr,2}$ and $f_{scr,3}$. For the diagonal crack C1 and C2, Eq. (23) can be used since $\ell_1 > \ell_t$ and the stress at cracks, $f_{scr,1}$ and $f_{scr,2}$, may be determined from Eq. (31).

$$f_{scr,1} = f_{scr,2} = E_s\left(\frac{w}{2.6\ell_k}\right) \le f_y \qquad (31)$$

For the crack C3 in Fig. 12, the behavior of the upper part of the shear reinforcement ℓ_2 is limited by the boundary conditions between cracks (f_s determined from Eq. (23)) while the behavior of the lower part ℓ_3 is controlled by the short unconfined bonded bar ($\ell < \ell_t$ and f_s determined with Eq. (13)). The stress at this crack $f_{scr,3}$ is therefore determined from the crack width for a typical RC member ($w \approx 1.3u_y$) from Eq. (32), where τ_b is limited by Eq. (27). To determined the debonding coefficient, k_d, it can be assumed that the bar slip along ℓ_2 is negligible when debonding occurs and s_ℓ can be replaced by w/1.3 from Eq. (15).

$$f_{scr,3} = \frac{4\ell\tau_b k_d}{d_b}\sqrt{1-\exp\left(\frac{f_{scr,3}\ell_k - 0.77wE_s}{E_s\alpha_{bp}}\right)} \le f_y \qquad (32)$$

Comparison of Behavior of Epoxy-Bonded Bars and Stirrups

Fig. 13 shows the behavior of post-installed epoxy-bonded shear reinforcement in terms of the axial bar stress as a function of the crack width determined from Eq. (31) and (32). Fig. 13 also compares the simplified model predictions to the detailed numerical predictions.

It can be seen that the simplified model provides a good prediction of the shear reinforcement behavior at a crack location compared to the detailed numerical model. For ℓ = 60 mm (2.36 in), a large crack (w > 1.4 mm, 0.055 in) is required to reach the maximum axial bar stress at the crack. For this short embedment length, the maximum stress is less than f_y. With a crack width, w, larger than 2.5 mm (0.098 in), the detailed numerical analysis predicts progressive debonding of the bar and consequently decreasing axial bar stresses. For a longer embedment length of 150

mm (5.91 in), the bar is predicted to have a stiffer response with the bar experience yielding at a crack width of 0.43 mm (0.017 in).

Fig. 14 indicates the predicted crack width at the maximum bar stress, $w_{fs,max}$, as a function of the embedment length for epoxy-bonded bars (Eq. (31) and (32)) in confined and unconfined conditions. These predictions are also compared with the predicted response for stirrups. For a very short embedment length, a large crack width $w_{fs,max}$ is required and debonding occurs. When ℓ equals ℓ_d in unconfined conditions, or when ℓ equals ℓ_{d0} in confined conditions, the epoxy-bonded bar yields without pullout. By comparing the bonded bar with the stirrups behavior illustrated in Fig. 14, it can be seen that $w_{fs,max}$ is larger for bonded bars than for stirrups for $\ell < \ell_d$. Between ℓ_{d0} and ℓ_t, $w_{fs,max}$ significantly decreases and the crack width at bar yielding approaches the crack width predicted for stirrups for $\ell > \ell_t$.

Comparison of Predictions with Results from Beam Tests

The previously proposed simplified model can be used to analyse the behavior of post-installed unconfined bonded bars in shear strengthened RC members. This type of shear strengthening as well as cast-in-place stirrups were used in beams tested by Cusson[4] and Provencher[3]. These beams were loaded up to shear failure and results were reported by Fiset *& al.*[5]. Fig. 15a presents the cracking pattern at shear failure and the location of the strain gauges on the shear reinforcing bars. Beam S1 contains cast-in-place stirrups and beams B1 and B2 contained post-installed epoxy-bonded shear reinforcement. For the shear reinforcement of these specimens, d_b = 16 mm (0.630 in), s_R = 0.6 d_b and f_R = 0.12 and the average material properties were: E_s = 200 GPa (29000 ksi), f_u = 630 MPa (91 ksi), ε_{sh} = 2%, ε_u = 18%, and τ_{b0} = 32.5 MPa (4700 psi).

348 Additional information about the beams specimens can be found in Fig. 15a as well as in Fiset &
349 *al.*[5]. Beams S1 and B1 were similar in terms of geometry and materials properties, but B1
350 experienced a shear capacity about 4% lower than S1 and 7% lower than the predicted shear
351 capacity for a member with stirrups according to the current standard CSA-S6[7]. Beam B2 with
352 bonded bars differs from beams S1 and B1 in terms of geometry and material properties. Its
353 experimental maximum shear capacity was 22 % lower than the predicted capacity of a member
354 with stirrups [7].

355 From the measured bar strain, the experimental axial bar stress at a crack, f_{scr}, may be
356 determined. However since the strain gauges were rarely positioned at the shear crack location,
357 Eq. (13) and (21) were used to extrapolate the strain at cracks to determine f_{scr} from Eq. (5)
358 (without strain hardening). From Eq. (31) and (32), the bar stress at a crack may also be
359 predicted according to the bar embedment length and the crack width. Fig. 15b presents the
360 experimental and the predicted f_{scr} corresponding to the crack width. For comparison purposes,
361 detailed numerical predictions are also presented.

362 From Fig. 15b, it is observed that the detailed numerical model and the simplified model provide
363 reasonable predictions of the shear reinforcement behavior. For beam S1 with stirrups, a small
364 crack width intersects bars R2 and R3 when these bars yield. The behavior of these stirrups is
365 well predicted by both models. For beam B1, the long embedment length of bar R3 enables the
366 bar to reach its yield strength for a small crack width similar to that of the stirrups in beam S1.
367 For bar R2 however, a small stress is observed due to the short embedment length at the lower
368 bar extremity. The detailed numerical and the simplified models predict maximum stresses at a

crack of 75 and 74 MPa (10.9 and 10.7 psi) respectively, while a maximum bar stress of 95 MPa (13.8 psi) was determined from the measured strains.

For the epoxy-bonded bars in beam B2 (Fig. 15b), the distance between the installed strain gauges and the diagonal crack is small. Fig. 15b shows that the bonded bar R3 reached its yield strength and the models provided good predictions. For bar R2, the maximum predicted bar stress at a crack is about 419 MPa (60.8 psi) and is close to the stress determined from the measured strains. At a crack width of about 1.2 mm (0.047 in), a secondary diagonal shear crack progressed and reached bar R2. This crack reduces by 22 mm (0.866 in) bar embedment length and caused a decreasing of the bar stress at the crack. By considering this cracking, bar pullout is well predicted by both models.

CONCLUSIONS

This paper presents a detailed numerical model used for predicting the bond behavior of post-installed epoxy-bonded bars and cast-in-place bars in terms of bond stress distribution, bar stress, bar slip and crack width. Simplified equations were developed to determine the axial bar stress developed at a shear crack corresponding to the shear crack width. The following conclusions are made from this research study:

1. Comparisons between the detailed numerical predictions, the results from simplified equations and the experimental pullout test results for cast-in-place reinforcing bars and epoxy-bonded bars indicated good agreement.

2. For epoxy-bonded bars, pullout tests and detailed numerical models have shown that the effect of yielding of the bonded bars on the bond strength seems to be less significant than

for cast-in-place bars due to the different bond mechanisms. However, this effect on epoxy-bonded bars should be investigated further to determine a more accurate Ω_y factor.

3. Both the detailed numerical model and the simplified model showed that the behavior of epoxy-bonded bars is greatly influenced by the embedment length. For embedment lengths shorter than the development length, a large crack is required to reach pullout and the bars stress is less than the bar yield strength. For embedment lengths greater than the development length, but smaller than a transition length, bar yielding can be attained only in the presence of a large crack. For embedment lengths greater than a transition length, the behavior of epoxy-bonded bars is similar to the behavior of cast-in-place stirrups and both types of bars exhibit a similar crack width at yielding.

4. Comparison of the predicted bar strain to the measured shear reinforcement strain in rectangular, simply-supported beams subjected to point loads, containing stirrups or post-installed epoxy-bonded shear reinforcement showed good agreement. The simplified model predicted pullout of epoxy-bonded bars having short embedment lengths and yielding of these bars having greater embedment lengths, as observed in beams reinforced with epoxy-bonded shear reinforcement.

ACKNOWLEDGMENTS

The authors gratefully acknowledge the funding from the Natural Sciences and Engineering Research Council of Canada (NSERC, CREATE-INFRA) and the “Fonds de Recherche du Québec – Nature et Technologies” (FRQNT).

REFERENCES

1. Johnson P. M., Couture A., Nicolet R., "Commission of Inquiry Into the Collapse of a Portion of the De La Concorde Overpass", Canada: Bibliothèque et Archives Nationales du Québec; 2007, 198 pp.

2. Mitchell D., Marchand J., Croteau P., Cook W. D., "Concorde Overpass Collapse: Structural Aspects", *Journal of Performance of Constructed Facilities*, V. 25, No. 6, 2011, pp. 545-553.

3. Provencher P., "Renforcement des dalles épaisses en cisaillement", Québec, Canada: Université Laval; 2010, 130 pp.

4. Cusson B., "Renforcement des dalles épaisses en cisaillement", Québec, Canada: Université Laval; 2012, 143 pp.

5. Fiset M., Bastien J., Mitchell D., "Methods for Shear Strengthening of Thick Concrete Slabs", *Journal of Performance of Constructed Facilities*, V. 31, No. 3, June 2017, pp. 10.

6. fib, "fib Model Code for Concrete Structures 2010", Lausanne, Switzerland: Ernst and Sohn; 2013, 653 pp.

7. CSA-S6, "Canadian Highway Bridge Design Code and Commentary", 11th ed. Mississauga, Canada: Canadian Standards Association; 2014, 1676 pp.

8. AASHTO, "LRFD Bridge Design Specifications 7th Ed. ", Washington US: American Association of State Highway and Transportation Officials; 2014, 2060 pp.

9. Fiset M., Bastien J., Mitchell D., "Experimental and Analytical Studies of Strengthening Using Drilled-in Bonded Shear Reinforcement", *Proceedings Structural Faults & Repair* 2014, London, UK, pp. 11.

10. Balazs G. L., "Cracking Analysis Based on Slip and Bond Stresses", *ACI Materials Journal*, V. 90, No. 4, Jul-Aug 1993, pp. 340-348.

11. Lee S. C., Cho J. Y., Vecchio F. J., "Tension-Stiffening Model for Steel Fiber-Reinforced Concrete Containing Conventional Reinforcement", *ACI Structural Journal*, V. 110, No. 4, Jul-Aug 2013, pp. 639-648.

12. Mahrenholtz C., "Seismic Bond Model for Concrete Reinforcement and the Application to Column-to-Foundation Connections", Stuttgart, Germany: Universität Stuttgart; 2012, 398 pp.

13. Jirsa J. O., Marques J. L., "A Study of Hooked Bar Anchorages in Beam-Column Joints", Report 33, University of Texas at Austin: Department of Civil Engineering; 1972, 92 pp.

14. Posey C. J., "Tests for Anchorages for Reinforcing Bars", Shearman M. Woodward ed. University Iowa City; 1933, 30 pp.

15. Brantschen F., "Influence of Bond and Anchorage Conditions of the Shear Reinforcement on the Punching Strength of RC Slabs", Lausanne, Switzerland: École Polytechnique Fédérale de Lausanne; 2016, 186 pp.

16. Brantschen F., Faria D. M. V., Fernández Ruiz M., Muttoni A., "Bond Behaviour of Straight, Hooked, U-Shaped and Headed Bars in Cracked Concrete", *Structural Concrete*, V. 17, No. 5, 2016, pp. 799-810.

17. Fernández Ruiz M., Muttoni A., Gambarova P. G., "Analytical Modeling of the Pre- and Postyield Behavior of Bond in Reinforced Concrete", *Journal of Structural Engineering*, V. 133, No. 10, 2007, pp. 1364-1372.

18. Lettow S., "Ein Verbundelement für nichtlineare Finite-Elemente-Analysen - Anwendung auf Übergreifungsstöße (Bond element for nonlinear finite element analysis - application to lap splices)", Stuttgart, Germany: University of Stuttgart; 2006, 206 pp.

19. Lowes L. N., Moehle J. P., Govindjee S., "Concrete-Steel Bond Model for Use in Finite Element Modeling of Reinforced Concrete Structures", *ACI Structural Journal*, V. 101, No. 4, July-Aug 2004, pp. 501-511.

20. ASTM-A996/A996M, "Standard Specification for Rail-Steel and Axle-Steel Deformed Bars for Concrete Reinforcement", A996/A996M-16, West Conshohocken, PA, USA: ASTM International; 2016, 5 pp.

21. Kankam C. K., "Relationship of Bond Stress, Steel Stress, and Slip in Reinforced Concrete", *Journal of Structural Engineering*, V. 123, No. 1, 1997, pp. 79-85.

22. Shima H., Chou L.-L., Okamura H., "Bond Characteristics in Post-Yield Range of Deformed Bars", *Doboku Gakkai Ronbunshu*, No. 378, 1987, pp. 213-220.

23. Villemure F.-A., Fiset M., Bastien J., Mitchell D., Fournier B., "Behaviour of Bonded Bars Post-Installed in Concrete Affected by Alkali-Silica Reaction", *ACI Materials Journal*, V. 116, No. 6, 2019, pp. 179-191.

24. Eligehausen R., Mallée R., Silva J. F., "Anchorage in Concrete Construction", Berlin, Germany: Ernst and Sohn; 2006, 391 pp.

25. Cosenza E., Manfredi G., Realfonzo R., "Behavior and Modeling of Bond of FRP Rebars to Concrete", *Journal of Composites for Construction*, V. 1, No. 2, 1997, pp. 40-51.

26. Eligehausen R., Cook R., Jorg A., "Behavior and Design of Adhesive Bonded Anchors", *ACI Structural Journal*, V. 103, No. 6, Nov-Dec 2006, pp. 822-831.

27. Cook R. A., Doerr G. T., Klingner R. E., "Bond Stress Model for Design of Adhesive Anchors", *ACI Structural Journal*, V. 90, No. 5, Sept-Oct 1993, pp. 514-524.

28. Cook R. A., Kunz J., Fuchs W., Konz R. C., "Behavior and Design of Single Adhesive Anchors under Tensile Load in Uncracked Concrete", *ACI Structural Journal*, V. 95, No. 1, Jan-Feb 1998, pp. 9-26.

29. McVay M., Cook R. A., Krishnamurthy K., "Pullout Simulation of Postinstalled Chemically Bonded Anchors", *Journal of Structural Engineering*, V. 122, No. 9, 1996, pp. 1016-1024.

30. Bentz E. C., Collins M. P., "Development of the 2004 CSA A23.3 Shear Provisions for Reinforced Concrete", *Canadian Journal of Civil Engineering*, V. 33, No. 5, 2006, pp. 521-534.

31. Rahal K. N., Collins M. P., "Background to the General Method of Shear Design in the 1994 CSA-A23.3 Standard", *Canadian Journal of Civil Engineering*, V. 26, No. 6, 1999, pp. 827-839.

32. Calvi P. M., "A Theory for the Shear Behaviour of Cracks Providing a Basis for the Assessment of Cracked Reinforced Concrete Structures", Toronto: University of Toronto; 2015, 346 pp.

33. Vecchio F. J., Lai D., "Crack Shear-Slip in Reinforced Concrete Elements", *Journal of Advanced Concrete Technology*, V. 2, No. 3, Oct 2004, pp. 289-300.

34. Vecchio F. J., Collins M. P., "The Modified Compression-Field Theory for Reinforced-Concrete Elements Subjected to Shear", *ACI Journal*, V. 83, No. 2, Mar-Apr 1986, pp. 219-231.

FIGURES

List of Figures:

Fig. 1 - a) Typical shear cracking pattern of a member with shear reinforcement and b) close-up of a bar pullout at shear crack location

Fig. 2 - a) Different types of embedded bars and boundary conditions in a shear cracked RC member, b) equilibrium of a bar element and expected axial bar stress, slip and bond stress distribution for c) a straight epoxy-bonded bar, d) a bar between 2 stabilized cracks and e) a hooked stirrup.

Fig. 3 - a) Types of stirrup anchorage, b) comparison of Eq. (4) with experimental test results [15] on U-shaped anchorages, bent bars and hooked bars ($f_{s0} \leq f_y$)

Fig. 4 - Flowchart for the detailed numerical model

Fig. 5 - a) Bond-slip relationship, b) bond strength reduction factor, Ω_y, for a cast-in-place bar (α = 0.85) and for an epoxy-bonded bar (α = 0.20)

Fig. 6 - Comparison of the detailed numerical model predictions with test results for a cast-in-place bar [21]: a) test setup, b) axial bar strain distribution at different load levels and c) relationship between axial bar $f_{s\ell}$ and average strain

Fig. 7 - Comparison of detailed numerical model predictions with test results on cast-in-place bars [22] a) test setup, b) axial bar stress response and c) axial bar strain distribution

513 Fig. 8 - Comparison of detailed numerical model predictions with test results on epoxy-bonded
514 bars [23]: a) test setup, b) average bond stress according to the bar slip and c) effect of the bar
515 yielding on the maximum epoxy-bonded bars capacities

516 Fig. 9 - Bar slip, bar stress and bond stress distribution along post-installed bonded bars, applied
517 stress $f_{s\ell} = f_y$

518 Fig. 10 - Detailed numerical model and simplified model predictions of a) the slip at the yielding
519 of epoxy-bonded bars as a function of the bar embedment length, b) axial bar stress as a function
520 of the slip of confined post-installed bonded bars (note: 1 mm = 0.0394 in, 1 MPa = 145 psi)

521 Fig. 11 - Pullout of confined and unconfined epoxy-bonded bars

522 Fig. 12 - a) Typical shear cracking and b) displacements and bar stress at a crack

523 Fig. 13 - Axial bar stress at a crack for an epoxy-bonded bar determined with the simplified
524 model and the detailed numerical model

525 Fig. 14 - Crack width at maximum axial bar stress as a function of the embedment length for a
526 stirrup and an epoxy-bonded bar (confined and unconfined conditions) (note: 1 mm = 0.0394 in,
527 1 MPa = 145 psi)

528 Fig. 15 - a) Cracking patterns and location of strain gauge in tested beams [5] and b), axial bar
529 stress at cracks determined from experiments and predicted by the detailed numerical model and
530 the simplified model (dimensions in mm, note: 1 mm = 0.0394 in, 1 MPa = 145 psi)

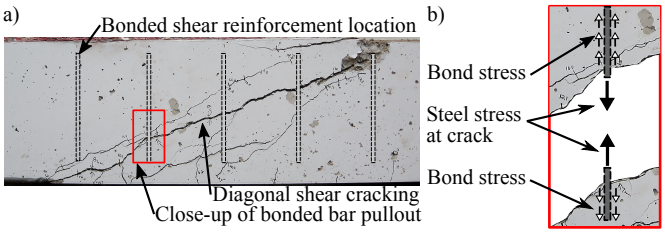

Fig. 1 – a) Typical shear cracking pattern of a member with shear reinforcement and b) close-up of a bar pullout at shear crack location

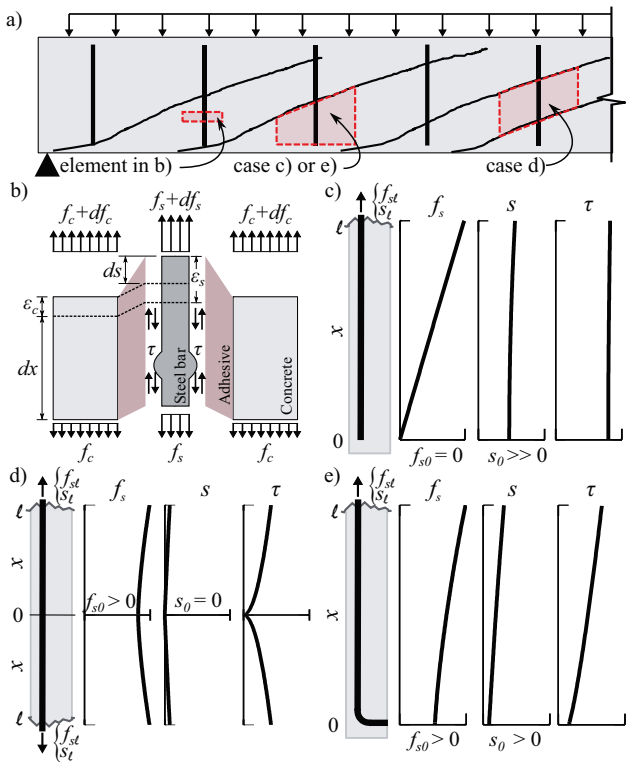

Fig. 2 – a) Different types of embedded bars and boundary conditions in a shear cracked RC member, b) equilibrium of a bar element and expected axial bar stress, slip and bond stress distribution for c) a straight epoxy-bonded bar, d) a bar between 2 stabilized cracks and e) a hooked stirrup

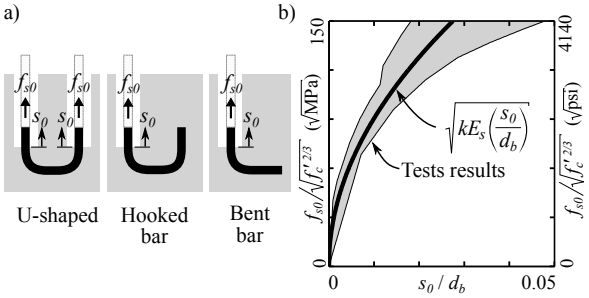

Fig. 3 – a) Types of stirrup anchorage, b) comparison of Eq. (4) with experimental test results [15] on U-shaped anchorages, bent bars and hooked bars ($f_{s0} \leq f_y$)

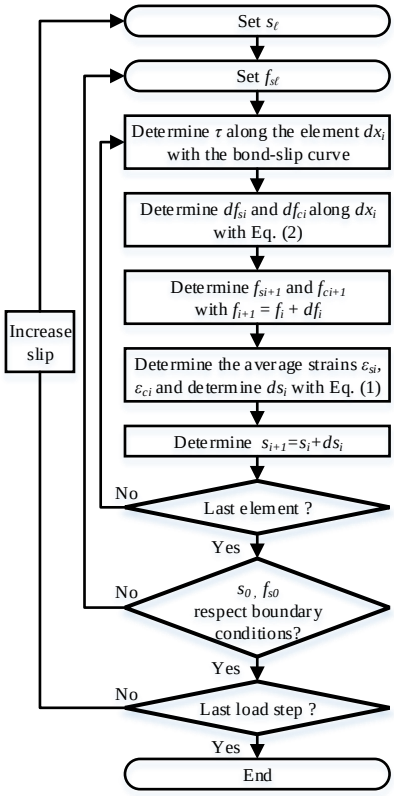

Fig. 4 – Flowchart for the detailed numerical model

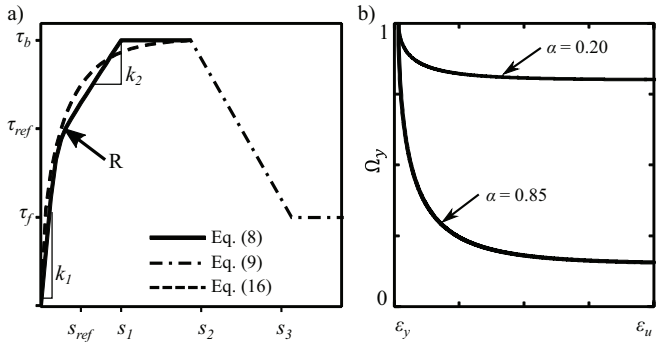

Fig. 5 – a) Bond-slip relationship, b) bond strength reduction factor, Ω_y, for a cast-in-place bar (α = 0.85) and for an epoxy-bonded bar (α = 0.20)

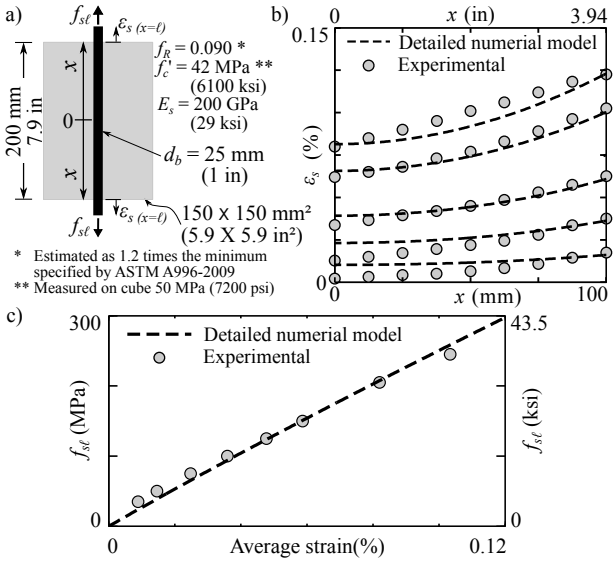

Fig. 6 – Comparison of the detailed numerical model predictions with test results for a cast-in-place bar [21]: a) test setup, b) axial bar strain distribution at different load levels and c) relationship between axial bar $f_{s\ell}$ and average strain

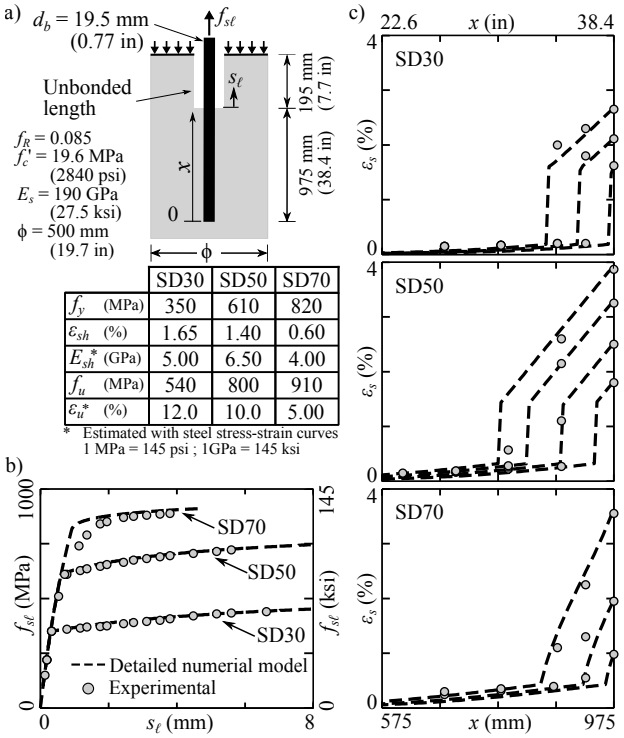

Fig. 7 – Comparison of detailed numerical model predictions with test results on cast-in-place bars [22] a) test setup, b) axial bar stress response and c) axial bar strain distribution

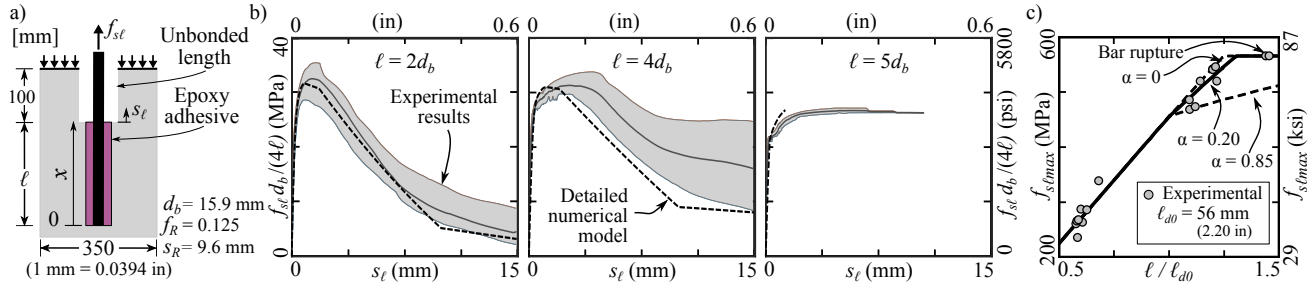

Fig. 8 – Comparison of detailed numerical model predictions with test results on epoxy-bonded bars [23]: a) test setup, b) average bond stress according to the bar slip and c) effect of the bar yielding on the maximum epoxy-bonded bars capacities

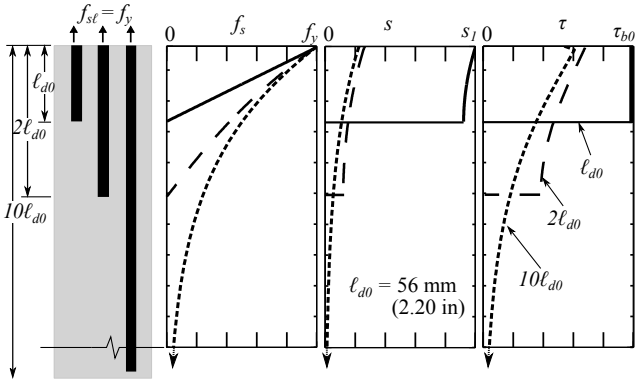

Fig. 9 – Bar slip, bar stress and bond stress distribution along post-installed bonded bars, applied stress $f_{s\ell} = f_y$

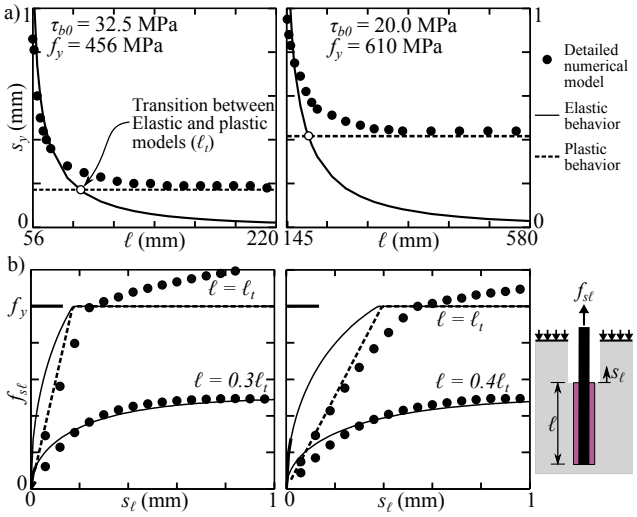

Fig. 10 – Detailed numerical model and simplified model predictions of a) the slip at the yielding of epoxy-bonded bars as a function of the bar embedment length, b) axial bar stress as a function of the slip of confined post-installed bonded bars (note: 1 mm = 0.0394 in, 1 MPa = 145 psi)

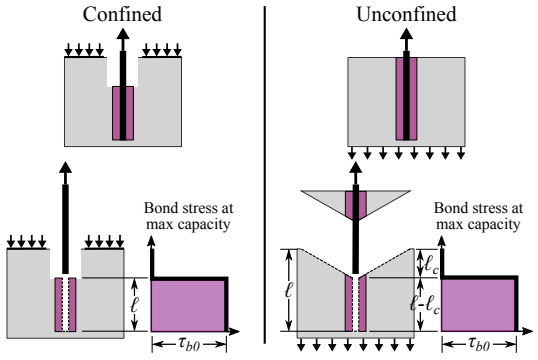

Fig. 11 – Pullout of confined and unconfined epoxy-bonded bars

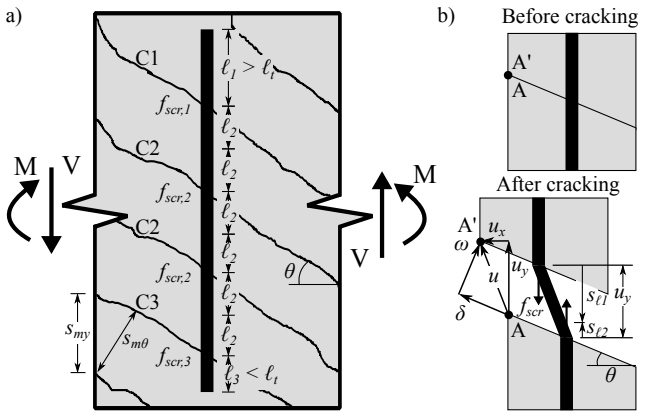

Fig. 12 – a) Typical shear cracking and b) displacements and bar stress at a crack

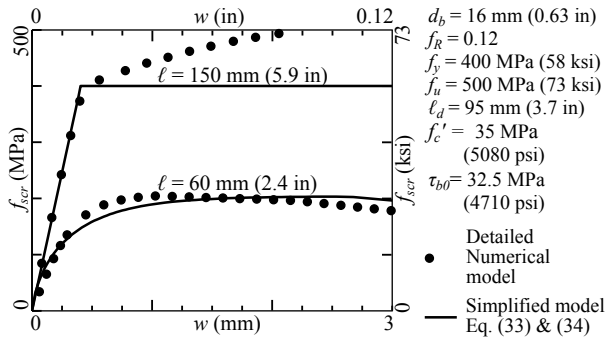

Fig. 13 – Axial bar stress at a crack for an epoxy-bonded bar determined with the simplified model and the detailed numerical model

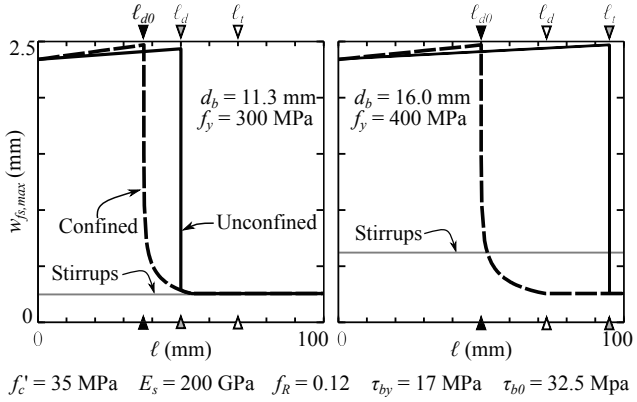

Fig. 14 – Crack width at maximum axial bar stress as a function of the embedment length for a stirrup and an epoxy-bonded bar (confined and unconfined conditions) (note: 1 mm = 0.0394 in, 1 MPa = 145 psi)

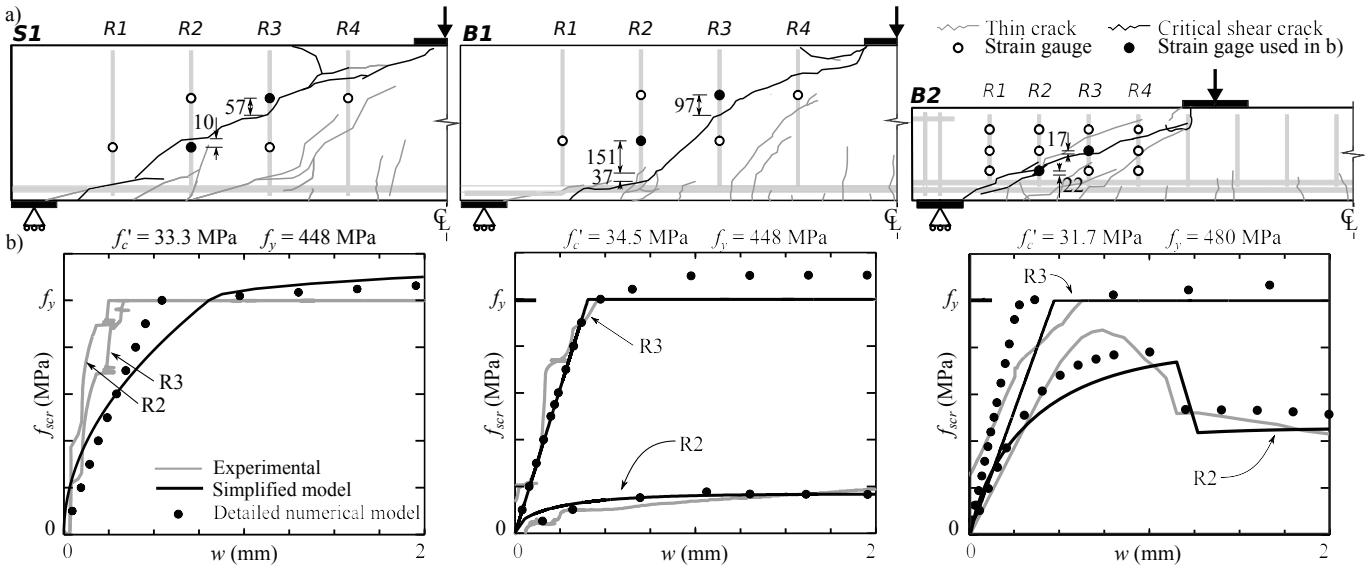

Fig. 15 – a) Cracking patterns and location of strain gauge in tested beams 5 and b), axial bar stress at cracks determined from experiments and predicted by the detailed numerical model and the simplified model (dimensions in mm, note: 1 mm = 0.0394 in, 1 MPa = 145 psi)